Passivity, dynamic performance and current limitation of MMC-based CC-GFM with harmonic filtering

Eros Avdiaj ⓘ, Dongyeong Lee ⓘ, Jie Song ⓘ, Marco Lindner ⓘ and Jef Beerten ⓘ

Abstract—Modern power systems are increasingly reliant on power electronics (PE), with high-power Modular Multilevel Converters (MMC)-based grid-forming (GFM) assets playing a vital role in ensuring voltage and frequency stability. However, time delays and fast controls of such devices compromise the system's stability due to their nonpassivities. Moreover, there is a proliferation of different PE-interfaced nonlinear loads that introduce harmonic distortions. To address these issues, MMC-based GFM converters might be required to provide harmonic filtering and exhibit passive behavior for stable interaction with other grid components.

Current saturation during faults or contingencies further complicates the operation of GFM converters, as it modifies dynamics and requires seamless transitions between current-limiting and GFM modes. Existing solutions are inadequate for current-controlled GFM (CC-GFM) structures, as they degrade passivity.

This paper proposes a seamless current limitation strategy for CC-GFM converters that preserves passivity and harmonic filtering during normal operation while ensuring stable and seamless transitions during current saturation. The approach freezes the states of the voltage feedforward and harmonic filtering compensators, enabling continuous output and bumpless transitions. Controller hardware in the loop experimental results validate the proposed method, highlighting its effectiveness in maintaining the current within the converter current limit.

Keywords—Current limitation, Frequency domain, Grid forming, MMC, Passivity

I. INTRODUCTION

Modern power systems are increasingly penetrated by power electronics converters in different voltage levels [1], the majority of which are voltage source converters (VSC). These converters are predominantly operated in grid-following (GFL) mode. However, grid-forming (GFM) converters emerge as valuable assets for future grids as they enhance the grid stiffness in terms of voltage and frequency [2]. This is especially critical for a grid dominated by power electronics as a result of phasing out conventional synchronous generators.

Apart from the voltage and frequency control, wide application of power-electronics-interfaced generators and loads also leads to emerging risks related to power/voltage quality as they are also considered as potential sources of harmonic current due to their nonlinear characteristics [3]. Such harmonic distortion may result in increased power losses and equipment damage. Also, undamped harmonics threaten the system stability [4]. Hence, recent requirements, in addition to GFM functionalities, are requesting GFM converters to provide harmonic filtering capabilities for the 5th, 7th, 11th, and 13th order harmonics [5].

Moreover, these requirements state that GFM assets should behave passively for frequency components not equal to the fundamental frequency (50Hz) in the stationary frame and contribute to the stable parallel connection of several converters and other network components [5]. Therefore, the VSC converter station with the GFM functionalities and harmonic filtering capabilities should be passive, thus ensuring no adverse interactions between the GFM asset and the rest of the power system should be ensured by design. This task is particularly challenging when considering Modular Multilevel Converters (MMC), which present large time delays compared to their increased switching frequency and have been shown to make the converter nonpassive and susceptible to harmonic instabilities[6].

Note that, unlike conventional synchronous generators, power converters have to saturate the current in case it is overloaded. Such current saturation modifies the converter operation by partially or fully disabling the outer control loop. As a result, the converter may exhibit significantly different dynamics when being saturated [7]. The grid-forming assets are expected to provide instantaneous short-circuit current contributions within the permissible current limits. The transition between the instantaneous current response and current limitation mode must be uninterrupted and as bumpless as possible [5]. Additionally, the recent grid-forming requirements [8] states that "in the event of reaching the current limitation, stable functioning and seamless transition back to voltage source mode is expected."

Various current saturation schemes have been presented in the literature for the GFM converters. Typical implementation includes current controller reference limitation [9], [10], insertion of transient virtual impedance [11], and voltage limiter [12]. The emerging stability issues resulting from the current-saturated operation of GFM converters have also been addressed in some references. Power-angle enhancement considering the converter's current limitation has been analyzed in [13]. The frequency instability risks related to the reduction of synthetic inertial from the GFM converters

in current-saturated operation have been pointed out in [14]. On the other hand, current saturation also imposes new challenges on the self-stability of GFM converter under disturbances such as synchronization [15] and anti-windup of the voltage controllers [16]. These investigations into transient stability are important, but another key challenge is to ensure robust stability during uncertain operation conditions, which is achieved by the passivity of the inner loops. There are no existing studies that examine both the passive behavior of the GFM with a current controller in the inner loops (CC-GFM) and its dynamic performance during faults.

It is well known that the dynamic performance of the current controlled VSC and their passivity properties are often conflicting objectives [17]. As it will be explained in this article, the current controller reference limitation does not satisfy the dynamic performance requirements to limit the converter current in case the GFM asset is designed to be passive. Several efforts have also been reported in the literature for GFL VSCs to develop new current saturation schemes that ensure both passivity and dynamic performance for current limitations [6], [17], [18], [19]. An engineering solution discussed in [6] involves enabling or disabling the voltage feedforward action based on the grid conditions. Specifically, the feedforward action is disabled in case of adverse harmonic interactions, thereby improving the dissipation properties of the converter and ensuring passivity. However, such a solution will result in discontinuities in the converter's output voltage, which are not desired. Another approach for GFL control strategies is to adjust the time constant of the voltage feedforward's first-order low-pass filter (LFP) in real-time. In this case, a slow LPF (big time constant) maintains the passivity properties of the admittance. While, during an overcurrent situation, the LPF time constant changes to a small value to ensure optimal current controller performance [18]. Additionally, the proposal in [19] suggests the current controller with the feedforward action but without an integration term in the current controller. Note that these approaches focus on GFL controls, and they are not effective for CC-GFM since they would result in reduced dissipation properties of the current controller, and the overall CC-GFM will result nonpassive.

This paper proposes a *seamless current limitation* strategy that maintains the passivity of CC-GFM's inner loops with harmonic filtering during normal operation and ensures safe converter operation during the current limitation mode. The uniqueness of this strategy lies in freezing the states of the voltage feedforward and harmonic filtering compensator, achieving a continuous converter output. This approach ensures stable functioning and a seamless transition between the current limiting mode and passive inherent GFM response.

The remainder of this paper is organized as follows. Section II presents the implications that the passivity-based design of the CC-GFM with harmonic filtering has on the converter's current limiting capabilities. The third section details the impact of the voltage feedforward on the passivity properties and on the current limiting capabilities. Section IV presents the proposed seamless current limitation strategy, followed by the experimental results in Section V. The paper concludes
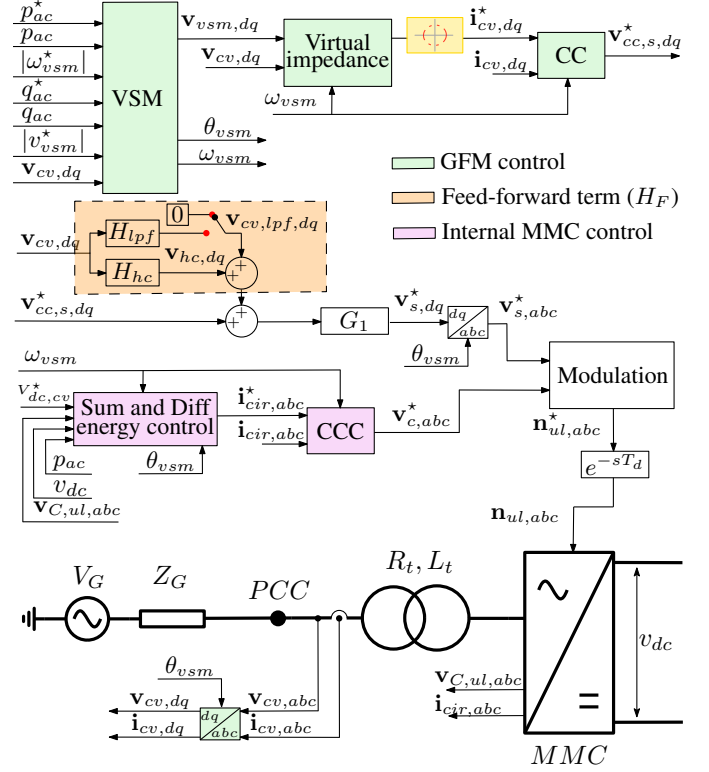

Fig. 1: MMC Equivalent Model and Proposed Control Scheme

with a summary of the findings in Section VI.

II. PASSIVITY-BASED DESIGN OF THE CC-GFM WITH HARMONIC FILTERING AND IMPLICATIONS IN CURRENT LIMITATION

The CC-GFM is designed to operate passively over a certain frequency range, which includes functionalities such as the voltage source behind impedance characteristic of the GFM control and harmonic filtering control. In order to mitigate harmonic interactions or converter-driven adverse interactions [20], a passivity-based design is preferred. These controllers are designed using a high-frequency GFM model and aim to maintain the passivity of the output admittance up to 2.5 kHz , as there are no requirements for the impedance of the GFM assets [8]. This section first presents the passivity theory and then discusses the implications of maintaining a passive converter admittance.

A. Passivity theory

The passivity of the $\mathbf{Y}_{dq}$ admittance matrix can be addressed in relationship to the power dissipation properties of the admittance [21]. The power dissipation at frequency ω are calculated as $P = \Re\{\mathbf{v}_d \mathbf{i}_d^* + \mathbf{v}_q \mathbf{i}_q^*\}$. Here $\mathbf{v}$ and $\mathbf{i}$ are the complex phasors at frequency ω. Moreover, in per unit quantities, P is equivalent to $1/2(\mathbf{v}^H \mathbf{i} + \mathbf{i}^H \mathbf{v})$, where the superscript H indicates the transpose and complex conjugate. Lastly, by considering $\mathbf{i} = \mathbf{Y}(j\omega)\mathbf{v}$, one can calculate P as

$$P = \frac{1}{2}(\mathbf{v}^H \mathbf{i} + \mathbf{i}^H \mathbf{v}) = \frac{1}{2}(\mathbf{v}^H [\mathbf{Y}(j\omega) + \mathbf{Y}^H(j\omega)]\mathbf{v}). \quad (1)$$

Therefore, if the matrix $[\mathbf{Y}(j\omega) + \mathbf{Y}^H(j\omega)]$ is positive definite, the power P is positive, thus for a load current convention (
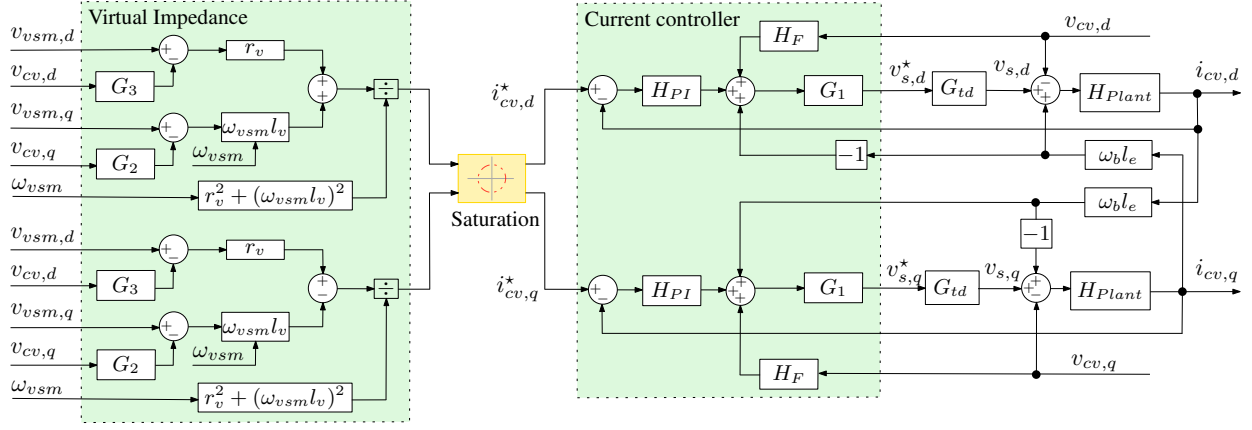
Fig. 2: Block diagram of the control and model of the MMC

TABLE I: Control parameters

Parameter	Value	Parameter	Value
ω_b	$2\pi \times 50$ rad/s	ω_{LPF,G_3}	$2\pi \times 66$ rad/s
$r_e, l_e/\omega_b$	0.016, $0.175/\omega_b$ pu	ξ_{G_3}	0.707
T_d	$100\,\mu s$	ω_{HPF,G_3}	$2\pi \times 2.41$ rad/s
$r_v, l_v/\omega_b$	0.01, $0.4/\omega_b$ pu	k_{hc}	2.08 pu
ω_{lead}	$2\pi \times 2.5 \times 10^3$ rad/s	a_{hc}	0.05
α_{lead}	$45°$	ϕ_{hc}	-1.706178 rad
ω_{LPF,G_2}	$2\pi \times 66$ rad/s	ω_h	$6 \times \omega_b$ rad/s
ξ_{G_2}	0.707	τ_{lpf}	0.16 ms

i.e. current that enters the device), the admittance dissipates energy at frequency ω [21]. If the power is dissipative for all frequencies then the converter system is passive. Lastly, $[Y(j\omega) + Y^H(j\omega)]$ is a Hermitian matrix, which has real eigenvalues, and we can calculate the dissipation directly by assessing the minimum eigenvalue of $[Y(j\omega) + Y^H(j\omega)]$. Note that the results of this indicator will be the same as the ones obtained evaluating $\Re(Y_{dd})$ if $Y_{dd} = Y_{qq}$ when $Y_{dq} = -Y_{qd} \approx 0$. However, in case $Y_{dq} = -Y_{qd} \neq 0$), the minimum eigenvalue of $[Y(j\omega) + Y^H(j\omega)]$ will provide the correct results regarding passivity.

B. Design of the passive CC-GFM

Fig.1 presents the full MMC-based CC-GFM based on [22]. To analyze the ac-side response, an ac-side high-frequency MMC model and control are presented in Fig. 2. The current reference of the virtual impedance is saturated to the magnitude of 1 pu. Therefore, we designed the converter to operate in two cases: unsaturated and saturated. The unsaturated case represents the response of the inner loops for CC-GFM as presented from all the blocks in Fig. 2 (without saturation block).

The different elements of the model are given below. G_{td} is the time delay model, H_{Plant} is the plant model and includes half the arm inductance and transformer, which is modeled as the rl branch. H_{PI} is the current controller. To maintain the passivity of the inner loops, several actions are needed, represented by G1, G2, and G3. G_1 is a lead-lag compensator that maintains passivity in the high frequency range and offset the impact of the time delay. G_2 and G_3 are the filters of the virtual impedance where both are second order low pass filets however G_3 in addition to the low pass filter has a high

pass filter that is utilized to increase the virtual resistance and improve the dissipation properties of the overall admittance of the converter.

$$G_{td} = e^{-T_d s}, \quad H_{Plant} = \frac{1}{r_e + s l_e}, \tag{2}$$

$$H_{PI} = k_p \frac{s + k_i/k_p}{s}, \tag{3}$$

$$G_1 = \frac{\beta_{lead} s + \omega_{lead}\sqrt{\beta_{lead}}}{s + \omega_{lead}\sqrt{\beta_{lead}}}, \quad \beta_{lead} = \frac{1 + \sin(\alpha_{lead})}{1 - \sin(\alpha_{lead})} \tag{4}$$

$$G_2 = \frac{\omega_{LPF,G_2}^2}{s^2 + 2\xi_{G_2}\omega_{LPF,G_2}s + \omega_{LPF,G_2}^2}, \tag{5}$$

$$G_3 = \frac{\frac{\omega_{LPF,G_3}^2}{\omega_{HPF,G_3}}s + \omega_{LPF,G_3}^2}{s^2 + 2\xi_{G_3}\omega_{LPF,G_3}s + \omega_{LPF,2}^2}, \tag{6}$$

Lastly, here H_F is the feed-forward compensator that includes the different feed-forward actions. For the passive CC-GFM with harmonic filtering,

$$H_F = H_{hc} = k_{hc}a_{hc}\frac{s\,\omega_h\,cos(\phi_{hc}) - (\omega_h)^2 sin(\phi_{hc})}{s^2 + a_{hc}\omega_h\,s + (\omega_h)^2}. \tag{7}$$

H_{hc} is the transfer function that provides harmonic filtering. where a_{hc} is the bandwidth, ϕ_{hc} is the compensation angle, k_{hc} is the gain of the compensator and lastly there is ω_h, which is the resonant frequency. This compensator can be used for several purposes. A high a_{hc} might be utilized for improve the dissipation properties in a wide frequency range [23] while a small a_{hc} can be utilized to introduce a resonant point for a particular harmonic of interest [19]. Finally, ϕ_{hc} is selected to maximize the dissipation of the admittance at the resonant point and ensure passivity [19].

Note that in the unsaturated model control, the GFM outer loops that generate the voltage magnitude and angle are limited to the lower frequency range. Moreover, the control of the internal dynamics of the MMC, such as circulating current and energy stored inside the MMC, are not modeled since they have negligible impact on the results in case compensated modulation is selected [22]. Fig. 3 presents the frequency domain validation of the $\mathbf{Y}_{dq}$ admittance matrix comparing the high-frequency model to a frequency sweep
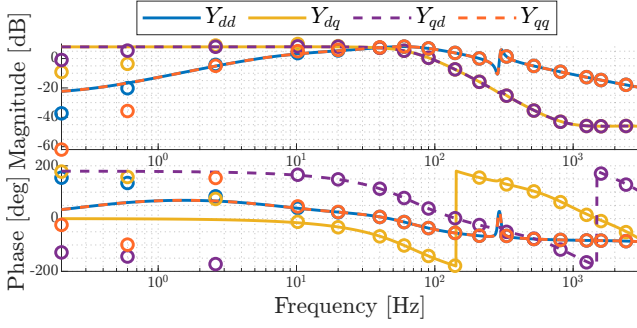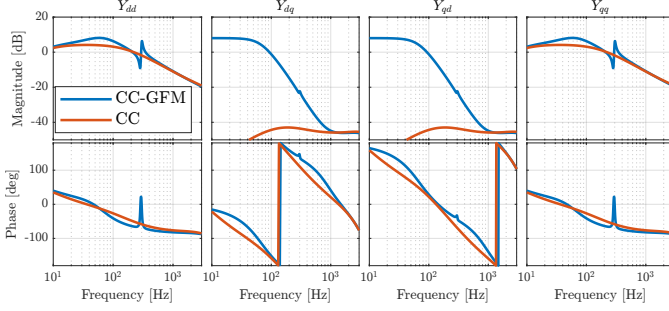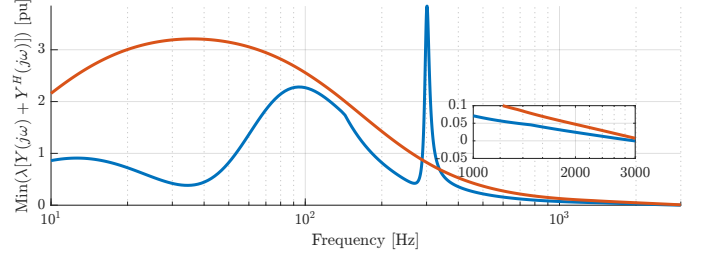
Fig. 3: Frequency domain validation

Fig. 4: $\mathbf{Y}_{dq}$ admittance matrix for normal state (CC-GFM) and saturated state (CC).

(a) **Without** voltage feed-forward action

(b) **With** voltage feed-forward action

Fig. 5: Dissipation properties $\mathbf{Y}_{dq}$ during normal state (CC-GFM) and saturated state (CC).

of the full CC-GFM MMC presented in Fig.1, which is implemented in an EMT software. The results indicated that the high-frequency model is valid above 10 Hz in the dq frame. Circles and lines of Fig. 3 denote the frequency sweep results and the responses of the developed model, respectively. The controls of the full CC-GFM MMC are based on [22] where the GFM outer loops are based on the virtual synchronous machine, while the MMC control utilizes a per-leg energy control as detailed in [22].

Simultaneously, the saturated state corresponds to the current controller response since the references are limited and assumed constant [19]. Additionally, during the saturated state, the harmonic filtering functionality is disabled, hence $H_{hc} = 0$. This is done in order to remove any possible harmonic current resulting as a consequence of the harmonic filtering, thus ensuring that the current remains within the limits which is maintained by the current controller.

Fig. 4 compares the converter's high-frequency admittance for the unsaturated and saturated state, named CC-GFM and CC, respectively. The control parameters are given in Tab. I. It is clear that the virtual impedance of the GFM control impacts the admittance. The virtual impedance has a significant impact in Y_{dq} and Y_{qd} while it has a reduced impact in Y_{dd} and Y_{qq}. Meanwhile, as expected, the harmonic filtering resonant terms impact Y_{dd} and Y_{qq}.

The dissipation properties of the admittance matrix for unsaturated and saturated cases are given in Fig. 5a. For the unsaturated case, the dissipation properties are high; therefore, the CC-GFM is passive. At the frequency of the harmonic filtering, the dissipation properties present a high peak, and close to the resonant point, the harmonic compensator does not introduce nonpassivities (which is due to the selection of
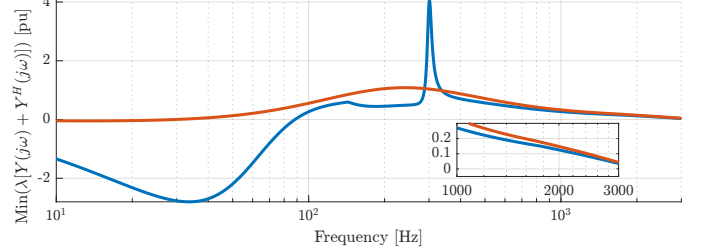
the compensation angle ϕ_{hc}).

It is important to note that to maintain passivity, there is no voltage feedforward in the dq-frame. As a result, the current limiting capability is impacted by the reduction in the voltage disturbance characteristics of the current controller [24]. In case the voltage feed-forward action is introduced to maintain the disturbance rejection characteristics of the current controller , the overall feed-forward compensation H_F is modified as,

$$H_F = H_{lpf} + H_{hc}, \tag{8}$$

where H_{lpf} is a first order low pass filter as $H_{lpf} = 1/(1 + \tau_{lpf}s)$, the admittance matrix of CC-GFM results nonpassive as can be seen in Fig. 5b. In the following section, we will assess the current limiting capabilities of the CC-GFM with and without a feed-forward action.

C. Current limiting capabilities

The current limitation is an important characteristic of the CC-GFM, which is related to the thermal capacity of MMC's IGBTs. The transistors usually have a maximum collector current of 2 pu for 1 ms. However, the thermal modeling for a half-bridge MMC submodule identified that the MMC can withstand only 1.3 pu for 1.5 s [25]. For transients shorter than 1 s, a slightly higher current than 1.3 pu is feasible; thus, an upper bound of 1.4 pu is considered in the following analysis.

Figure 6 presents the current limitation capability of the CC-GFM for two cases named Case 1 and Case 2. The current limitation is demonstrated for a three-phase-to-ground fault applied at the PCC for 130ms, and the fault impedance is 0.01 pu. The time domain responses are based on the full CC-GFM presented in Fig. 1 where in Case 1, CC-GFM does not have a voltage feedforward ($\mathbf{v}_{cv,lpf} = 0$) hence the ac side admittance has passive inner loops. Meanwhile, Case 2 has a voltage feed-forward, which results in the nonpassive converter. i_{limit}, in Fig. 6, indicates the maximum permissible current of 1.4 pu.
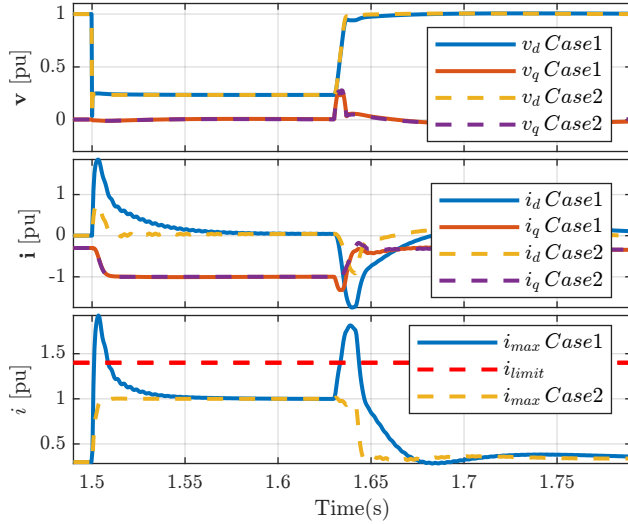
Fig. 6: GFM-MMC response to three phase to ground fault for Case 1 (passive CC-GFM without feedforward) and Case 2 (nonpassive CC-GFM with feedforward).

(a) Bode of $\mathbf{Y}_{dd}$

(b) Real part of $\mathbf{Y}_{dd}$

(c) I_d response to step in V_d

(d) I_d response to step in $I_d^{\star}$

Fig. 7: Comparison of the current controller loops for three cases, i) PI, ii) PI with feed-forward FF action, iii) P with feed-forward action.

III. IMPACT OF THE VOLTAGE FEEDFORWARD ACTION IN PASSIVITY AND CURRENT LIMITING CAPABILITIES

In the results presented in Fig. 6, the q-axis converter current i_q is similar with and without the voltage feed-forward action while the d-axis converter current i_d is different. This happens since the fault is seen as a perturbation in the voltage magnitude and $V_d \approx V_{mag}$. Therefore the response of $i_d = Y_{dd}v_d$ while $i_q = Y_{qd}v_d$. During the unsaturated case, i_q will respond depending on Y_{dq} for CC-GFM (see Fig. 5) the current will increase until the saturation is reached and it will stop changing since Y_{dq} for the saturated state is negligible. The feed-forward action will not impact Y_{dq} as long as the current controller in the dq-frame is decoupled; thus, i_q will have the same response whether there is a voltage feed-forward or not. Meanwhile, Y_{dd} will be directly impacted by the voltage feed-forward during both saturated and unsaturated states.

To analyze the impact of voltage feedforward action on passivity and current limiting capabilities of the current controller (which correspond to the saturated state), we will compare the Y_{dd} admittance in three scenarios:

1) Current controller PI without feedforward (PI): This configuration is passive but exhibits poor dynamic performance.
2) Current controller PI with feedforward (PI+FF): This setup offers good dynamic performance but is nonpassive.
3) Current controller P with feedforward (P+FF): This arrangement also provides good dynamic performance while remaining passive.
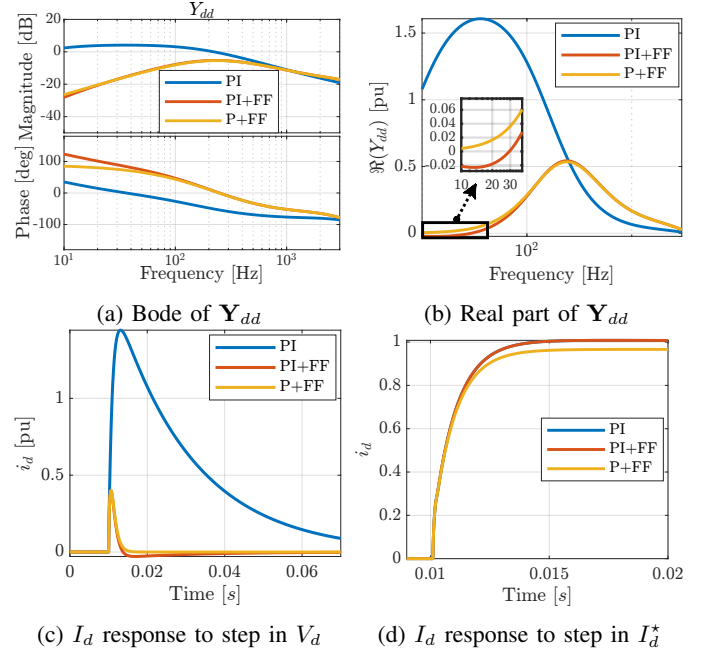
The current controller with feedforward (PI or P with FF) demonstrates superior disturbance rejection capabilities. This is evident in Fig.7a, where the admittance magnitude in Y_{dd} is smaller in case there is a feedforward action. A smaller admittance magnitude means less current reaction to voltage disturbances. This is evident in Fig.7c, which gives the step response of the Y_{dd}, indicating that the CC with FF quickly returns the current to its steady-state value. Nevertheless, the dissipation properties of the CC are highly reduced. The dissipation properties for the saturated case can be evaluated by the real part of Y_{dd} admittance, presented in Fig.7b, since $Y_{dq} \approx 0$ in the saturated state. One can notice that if there is no feed-forward action, the dissipation properties are highly improved, which, in consequence, makes the inner loops of the CC-GFM passive. Note that the controller with only a proportional gain and feedforward (P+FF) is passive and exhibits good disturbance rejection. While P+FF would have resulted in a solution for GFL controls, this is not the same for CC-GFM controls.

Lastly, the closed-loop response of the current controller is tuned identically for all configurations, as shown in Fig. 7d, which gives the step response of the current controller. Therefore, any observed slow response is primarily due to the lack of disturbance rejection in the CC. Based on this analysis, it is recommended to disable the feedforward action during normal operation. Instead, the feedforward action should be enabled only when the system is in a saturated state.

IV. SEAMLESS CURRENT LIMITATION STRATEGY

During severe transients, a specialized current limiting strategy is essential. In this paper, we propose a seamless current limitation strategy that is based on the freezing of the states within the feed-forward actions which includes
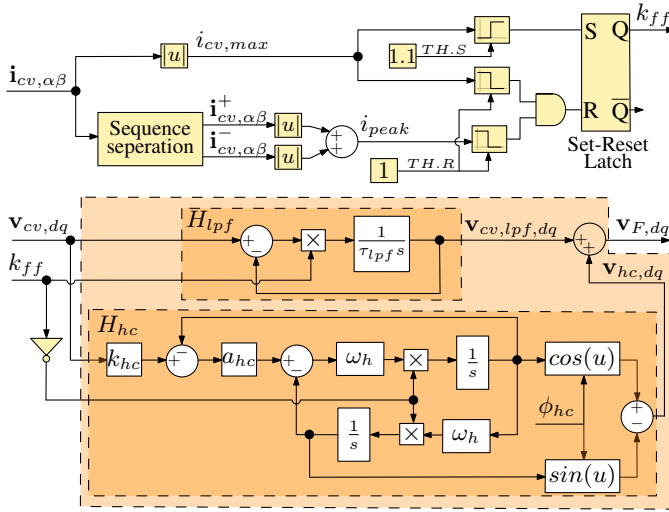
Fig. 8: Current limitation strategy.

Fig. 9: Set-up for Hardware in the Loop experiment.

both H_{lpf} and H_{hc}. By doing so, the control design can simultaneously ensure requirements and functionalities, such as passivity-based design with harmonic filtering, while achieving a seamless current limitation strategy. In addition to the saturation of the current reference magnitude at 1 pu, the proposed high-level current limitation strategy is presented in Fig. 8.

The current limitation strategy is enabled by a Set-Reset Latch logic port. When the instantaneous current magnitude $i_{cv,max}$ reaches a magnitude higher than the Threshold Set (TH.S) of 1.1 pu, the latch is set thus $k_{ff} = 1$. When the peak current i_{peak} and $i_{cv,max}$ are less than a Threshold Reset (TH.R) of 1 pu the latch is reset and $k_{ff} = 0$. The current $i_{cv,max}$ is the instantaneous maximum current, whereas the current i_{peak} is the expected peak current, and it is calculated by summing the fundamental positive and negative sequence current magnitudes as illustrated in the top part of Fig. 8 thus it remains constant and above 1pu in case of unbalanced fault scenarios. The calculation of i_{peak} is based after [26]. The gain k_{ff} determines the enabling and disabling of the voltage feed-forward action and harmonic compensator, respectively. When $k_{ff} = 1$, the voltage feedforward integration action unfreezes while the harmonic compensator freezes. Conversely, when $k_{ff} = 0$, the voltage feedforward freezes, and the harmonic compensator unfreezes.

For example, on the one hand, during normal operation, both i_{peak} and $i_{cv,max}$ are less than 1 pu, resulting in $k_{ff} = 0$. Under these conditions,

$$\mathbf{v_{cv,lpf}} = \int \frac{k_{ff}}{\tau_{lpf}} (\mathbf{v_{cv}} - \mathbf{v_{cv,lpf}}) dt \quad k_{ff} = 0, \quad (9)$$

the state of the feed-forward low pass filter remains unchanged and does not influence the system's dynamics. Consequently, from a small signal perspective, the dissipation properties of CC-GFM are maintained. Simultaneously, based on Fig. 8, the dynamics of the harmonic compensator persist, thus maintaining the desired functionalities of the asset. On the other hand, when $i_{cv,max} > 1.1$ pu, the current
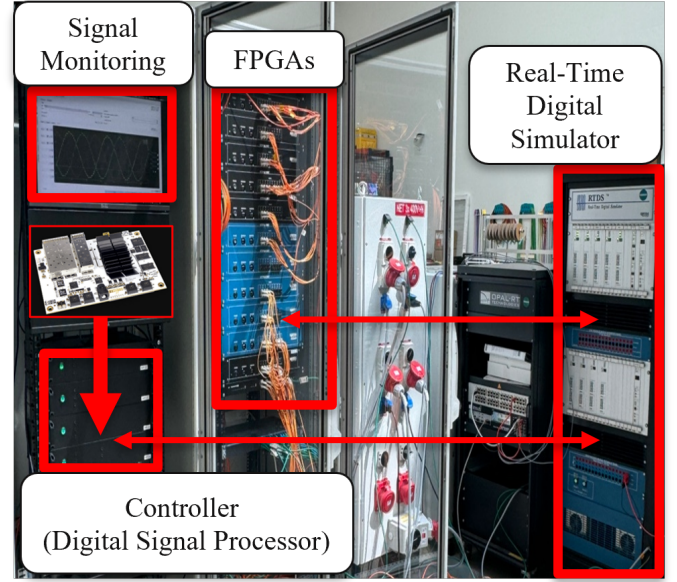
limiting strategy is enabled and the states of the harmonic conpensator are frozen. Consequently, the dynamics of the voltage feed-forward are enabled, thus maintaining the desired dynamic performance of the current controller and ensuring the safe operation of the converter. The current limitation strategy will persist until the Latch is reset (i.e., both i_{peak} and $i_{cv,max}$ are less than TH.R).

V. EXPERIMENTAL RESULTS

The experimental results present the controller hardware in-loop (C-HIL) validation of the proposed control structure. The C-HIL setup follows the latest recommendations for HVDC control and protection studies [27]. It includes a Digital Signal Processor (DSP) with an FPGA, Xilinx Zynq XC7Z030-3FBG676E, and a processor, 2x ARM Cortex A9 1 GHz, for the proposed controller. Additionally, a Real-Time Digital Simulator (RTDS) is employed for the main power system environment, connected with FPGAs for simulating detailed switching circuits of the MMC arms with Sub-Modules (SM), SM sorting algorithm, and IGBT firing. This configuration is illustrated in Fig. 9. This experimental setup evaluates the voltage source behavior and seamless current limitation under a grid voltage phase jump, three-phase-to-ground fault, and single-line-to-ground fault.

1) Response with to $30°$ jump in grid voltage phase: One of the tests to characterize the instantaneous current response of the voltage source behind impedance behavior of GFM controls is a phase jump in the grid voltage. Figure 10 presents the PCC's currents and voltages and the current limiting strategy signal (k_{ff}) in the case of a $30°$ phase jump in the grid voltage. The operating point before the perturbation is P=0.8 pu and Q=0pu.

During the initial transient, the current maximum i_{max} increases to 1.1 pu, thus k_{ff} goes from 0 to 1, activating the dynamics of the voltage feed-forward and deactivating the dynamics of the harmonic compensator control. Once i_{max}
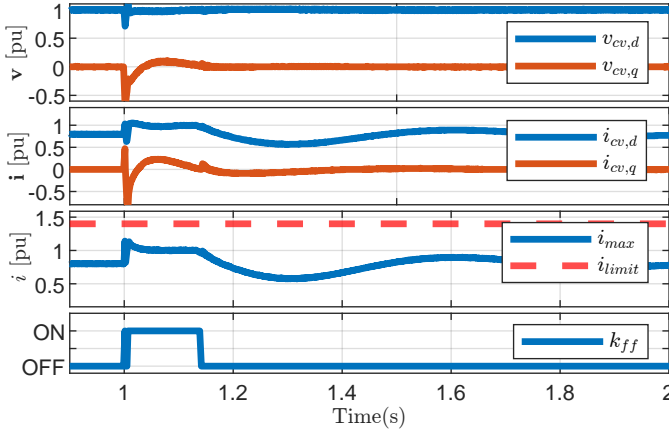
Fig. 10: Time response with respect to $30°$ phase jump.

and i_{peak} return within 1 pu, the control leaves the current limiting strategy and returns to normal operations (k_{ff} goes from 1 to 0). The transition between the current limitation and normal operation is seamless with the proposed controller.

2) Response with three-phase-to-ground fault: In this scenario, a three-phase-to-ground fault is incepted at the PCC through a fault impedance of 0.01 pu. The fault lasts for 130ms, after which it is cleared. The pre-fault operating point is P=0.95 pu and Q=0 pu. Fig. 11 presents the voltage and current magnitude, current peak at the PCC, the current limiting strategy state evaluated by k_{ff} and the output voltage of the low pass filter $v_{cv,lpf}$ and harmonic compensator v_{hc} (see Fig. 8).

Fig. 11 presents two cases, Case 1 (C1) and Case 2 (C2). C1 is the approach based on [6] that disables the output of the voltage feed-forward without freezing the low-pass filter integrator state, while C2 is the proposed strategy that freezes the integrator state. The triggering signal logic is the same for both cases based on the upper part of Fig. 8. Note that enabling the output of the voltage according to C1 does not maintain the current within the limit ($i_{max} > 2$ pu). Meanwhile, with C2, the current is maintained within the limit. After the fault is cleared, there is maximum power transfer to re-synchronize the virtual synchronous machine with the grid. Once the synchronization happens, the current returns to normal operation. During the transition from the current limitation strategy to normal operation, C1 presents high discontinuities in the feed-forward output voltages, $v_{cv,lpf}$ and v_{hc}, while C2 does not. The oscillations present in v_{hc} for C2 happen when the current limitation strategy is disabled, and the change in the grid voltage input impacts the internal states of the harmonic compensator since k_{ff} returns to 0. The damping of these oscillations and the time to reach the new steady state depends on a_{hc}.

3) Response with single-phase-to-ground fault: This subsection considers a single-phase-to-ground fault where the pre-fault operating point is P=0 pu and Q=0.95 pu. The single-phase-to-ground fault introduces unbalances in the three-phase system, which consequently introduces 100 Hz oscillations in the voltage and current maximum. While i_{max} enables the current limitation strategy, i_{peak} remains higher than 1, thus maintaining the current limitation strategy.
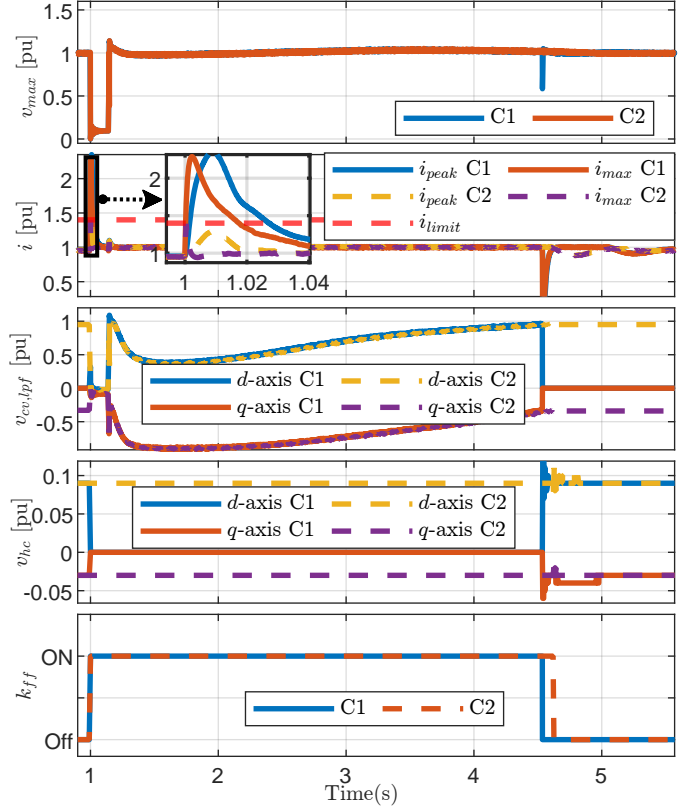

Fig. 11: Time response with respect to three-phase fault.

Similarly, as before, the current limit is violated for C1, and there are discontinuities in the output of the converter voltage. Meanwhile, the proposed current limitation strategy maintains the current within limits and seamlessly transitions between the current limitation strategy and normal operation.

VI. CONCLUSION

This paper presented a current-saturation scheme for a CC-GFM converter with harmonic filtering capabilities. A passivity-based design is adopted for the harmonic filtering and GFM control, thus fulfilling the harmonic filtering and passivity requirements. However, the passivated CC-GFM does not meet the current limitation requirements. Therefore, a seamless current limiting strategy is proposed to improve the converter's dynamics under disturbances (e.g., short-circuit faults).

In particular, a set-reset-latch strategy has been developed to activate/freeze the voltage and harmonic compensator feed-forward actions. The set-reset-latch triggering signal considers the instantaneous current magnitude to quickly limit the current during the fault and to ensure a smooth recovery to normal operating mode after the fault clearance. The effectiveness of the proposed control has been validated through controller-HIL tests involving different fault scenarios. Future investigations can be carried out to extend the current saturation scheme to CC-GFM converters with different control implementations.
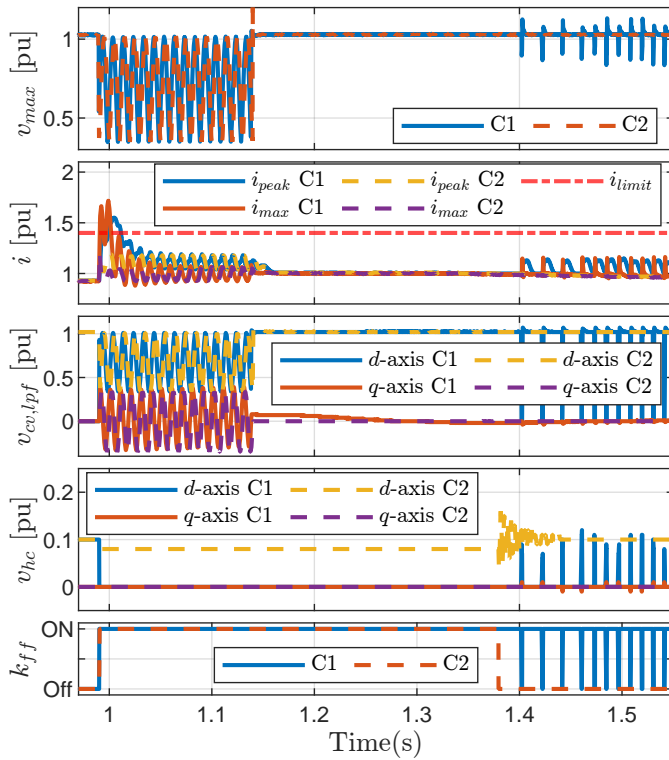
Fig. 12: Time response with respect to single-phase fault.

References

[1] S. Peyghami, P. Palensky, and F. Blaabjerg, "An overview on the reliability of modern power electronic based power systems," *IEEE Open Journal of Power Electronics*, vol. 1, pp. 34–50, 2020.

[2] R. H. Lasseter, Z. Chen, and D. Pattabiraman, "Grid-forming inverters: A critical asset for the power grid," *IEEE Journal of Emerging and Selected Topics in Power Electronics*, vol. 8, no. 2, pp. 925–935, 2020.

[3] CIGRE WG B4.67, "AC side harmonics and appropriate harmonic limits for VSC HVDC," https://www.e-cigre.org/publications/detail/754-ac-side-harmonics-and-appropriate-harmonic-limits-for-vsc-hvdc.html, 2019.

[4] N. G. M. Thao, K. Uchida, K. Kofuji, T. Jintsugawa, and C. Nakazawa, "An automatic-tuning scheme based on fuzzy logic for active power filter in wind farms," *IEEE Transactions on Control Systems Technology*, vol. 27, no. 4, pp. 1694–1702, 2019.

[5] 50herts, Amprion, Tennet, TransnetBW, "4-tso paper on requirements for grid-forming converters," Germany, Tech. Rep., 2024.

[6] G. Li, W. HUANG, H. RAO, Y. Li, S. XU, C. ZOU, and J. FENG, "A new high-frequency resonance suppression strategy for vsc-hvdc system," in *CIGRE Paris session 2022*, 2022, p. 10316.

[7] K. V. Kkuni, M. Nuhic, and G. Yang, "Power system stability impact assessment for the current limits of grid supporting voltage-source converters," in *2021 IEEE Power and Energy Society General Meeting (PESGM)*, 2021, pp. 1–5.

[8] ENTSO-E, "Grid forming capability of power park modules: First interim report on technical requirements," European Network of Transmission System Operators for Electricity (ENTSO-E), Tech. Rep., May 2024. [Online]. Available: https://www.entsoe.eu/Documents/Publications/SOC/20240503_First_interim_report_in_technical_requirements.pdf

[9] M. G. Taul, X. Wang, P. Davari, and F. Blaabjerg, "Current limiting control with enhanced dynamics of grid-forming converters during fault conditions," *IEEE Journal of Emerging and Selected Topics in Power Electronics*, vol. 8, no. 2, pp. 1062–1073, 2020.

[10] T. Qoria, X. Wang, and R. Kadri, "Grid-forming control vsc-based including current limitation and re-synchronization functions to deal with symmetrical and asymmetrical faults," *Electric Power Systems Research*, vol. 223, p. 109647, 2023.

[11] X. Xiong, C. Wu, and F. Blaabjerg, "Effects of virtual resistance on transient stability of virtual synchronous generators under grid voltage sag," *IEEE Transactions on Industrial Electronics*, vol. 69, no. 5, pp. 4754–4764, 2022.

[12] B. Fan, T. Liu, F. Zhao, H. Wu, and X. Wang, "A review of current-limiting control of grid-forming inverters under symmetrical disturbances," *IEEE Open Journal of Power Electronics*, vol. 3, pp. 955–969, 2022.

[13] L. Huang, H. Xin, Z. Wang, L. Zhang, K. Wu, and J. Hu, "Transient stability analysis and control design of droop-controlled voltage source converters considering current limitation," *IEEE Transactions on Smart Grid*, vol. 10, no. 1, pp. 578–591, 2019.

[14] B. Shakerighadi, N. Johansson, R. Eriksson, P. Mitra, A. Bolzoni, A. Clark, and H.-P. Nee, "An overview of stability challenges for power-electronic-dominated power systems: The grid-forming approach," *IET Generation, Transmission & Distribution*, vol. 17, no. 2, pp. 284–306, 2023. [Online]. Available: https://ietresearch.onlinelibrary.wiley.com/doi/abs/10.1049/gtd2.12430

[15] T. Qoria, F. Gruson, F. Colas, G. Denis, T. Prevost, and X. Guillaud, "Critical clearing time determination and enhancement of grid-forming converters embedding virtual impedance as current limitation algorithm," *IEEE Journal of Emerging and Selected Topics in Power Electronics*, vol. 8, no. 2, pp. 1050–1061, 2020.

[16] B. Fan and X. Wang, "Fault recovery analysis of grid-forming inverters with priority-based current limiters," *IEEE Transactions on Power Systems*, vol. 38, no. 6, pp. 5102–5112, 2023.

[17] L. Harnefors, H.-P. Nee, and M. Bongiorno, "Frequency-domain passivity-based current controller design," *IET Power Electronics*, vol. 1, no. 1, pp. 1–11, 2008.

[18] L. Harnefors and M. Bongiorno, "Current controller design for passivity of the input admittance," in *2009 13th European Conference on Power Electronics and Applications*, 2009, pp. 1–8.

[19] L. Harnefors, A. G. Yepes, A. Vidal, and J. Doval-Gandoy, "Passivity-based controller design of grid-connected vscs for prevention of electrical resonance instability," *IEEE Transactions on Industrial Electronics*, vol. 62, no. 2, pp. 702–710, 2015.

[20] N. Hatziargyriou, J. Milanovic, C. Rahmann, V. Ajjarapu, C. Canizares, I. Erlich, D. Hill, I. Hiskens, I. Kamwa, B. Pal, P. Pourbeik, J. Sanchez-Gasca, A. Stankovic, T. Van Cutsem, V. Vittal, and C. Vournas, "Definition and classification of power system stability – revisited & extended," *IEEE Transactions on Power Systems*, vol. 36, no. 4, pp. 3271–3281, 2021.

[21] L. Harnefors, M. Bongiorno, and S. Lundberg, "Input-admittance calculation and shaping for controlled voltage-source converters," *IEEE Transactions on Industrial Electronics*, vol. 54, no. 6, pp. 3323–3334, 2007.

[22] E. Avdiaj and J. Beerten, "Optimal control selection for grid-forming mmc-based assets: An analysis of interplay between gfm and internal mmc controls," in *CIGRE Paris session 2024*, 2024, p. 11895.

[23] E. Avdiaj and J. Beerten, "Time delay-induced control cross-coupling in vsc-mmc systems: Implications in harmonic mitigation, passivity and stability," in *2024 IEEE Power and Energy Society Innovative Smart Grid Technologies Conference (ISGT)*, 2024, pp. 1–6.

[24] A. Yazdani and R. Iravani, *Control of Half-Bridge Converter*. Wiley-IEEE Press, 2010, pp. 48–68.

[25] P. D. Judge and T. C. Green, "Dynamic thermal rating of a modular multilevel converter hvdc link with overload capacity," in *2015 IEEE Eindhoven PowerTech*, 2015, pp. 1–6.

[26] E. Avdiaj, J. Are Suul, S. D'Arco, and L. Piegari, "A current controlled virtual synchronous machine adapted for operation under unbalanced conditions," in *2020 9th International Conference on Renewable Energy Research and Application (ICRERA)*, 2020, pp. 263–270.

[27] G. Wang, "Guide to develop real-time simulation models for hvdc operational studies," *DC systems and power electronics (B4), Cigre*, no. 864, pp. 1–167, Feb 2022.